Journal of Constructional Steel Research 130 (2017) 65–78

Contents lists available at ScienceDirect

Journal of Constructional Steel Research

Investigation of an articulated quadrilateral bracing system utilizing shape memory alloys

Matthew S. Speicher [a,*,1], Reginald DesRoches [b], Roberto T. Leon [c]

[a] National Institute of Standards and Technology, 100 Bureau Drive, Gaithersburg, MD, United States
[b] School of Civil & Environmental Engineering, Georgia Institute of Technology, 790 Atlantic Drive, Atlanta, GA 30332-0355, United States
[c] Department of Civil & Environmental Engineering, Virginia Polytechnic Institute and State University, 102-D Patton Hall, Virginia Tech, Blacksburg, VA 24061, United States

ARTICLE INFO

Article history:
Received 9 June 2016
Received in revised form 22 November 2016
Accepted 24 November 2016
Available online 12 December 2016

Keywords:
Shape memory alloys
NiTi
Recentering
Seismic retrofit
Braced frame
Tension bracing

ABSTRACT

A shape memory alloy based articulated quadrilateral bracing system is developed and experimentally tested for seismic resisting applications. The articulated quadrilateral arrangement provides a scalable, reconfigurable, convenient means of combining nickel-titanium (NiTi) wires and energy dissipating elements. This configuration creates a system with an adjustable amount of recentering and damping, which could potentially be used in a wide variety of new and existing buildings. For these prototype tests, NiTi wire bundles were combined with long C-shaped dampers to create a system with a good balance of recentering and energy dissipation. The system was subjected to cyclic loading to assess the behavior. The system maintained strength, ductility, and recentering after being cycled to 2% drift, which is a typical maximum in structural systems if non-structural elements are to be preserved. An analytical case study demonstrated that shape memory alloy systems tend to distribute the deformation more evenly over the height of the structure compared to traditional systems, which is a desirable seismic performance characteristic. It is envisioned that, by using the same basic bracing setup, a wide range of force-deformation responses can be at an engineer's disposal.

Published by Elsevier Ltd.

1. Introduction

This study presents the design and proof-of-concept testing of a shape memory alloy (SMA)-based recentering articulated quadrilateral (AQ) bracing system. The 1994 Northridge and 1995 Kobe earthquakes revealed deficiencies in a large number of welded moment frames [1], which were previously held as the "gold-standard" in terms of ductile seismic behavior. This unexpected performance under moderate earthquake shaking resulted in a reevaluation of the seismic integrity of steel moment resisting frames. Moreover, researchers began to revisit other lateral load resisting systems, giving the engineering community new options in earthquake-resistant design.

Braced frames are one of the main viable alternatives to moment resisting frames. To obtain the desired level of ductility, traditional braced frame systems are designed with special attention to the connections, slenderness ratios, and width-to-thickness ratios of the braces, as well as to the effect of brace overstrength on adjacent members [2]. However, even with these special measures, traditional braces are characterized by a loss of load carrying capacity due to buckling and by degrading behavior and fracture due to low-cycle fatigue and strain localization.

To achieve improved performance, newer systems, such as buckling-restrained braced frames (BRBFs), have become attractive and popular options. The BRBF performance is generally characterized by a buckling-restrained brace (BRB) with an elastoplastic-type response in both tension and compression. The BRB generally has reliable energy dissipation, controlled strength, and excellent ductility. Though the BRBF has been shown to have a high level of performance, it provides no specific mechanism with which to reduce residual drifts of a structure; which may be the determining factor in whether a damaged building can be repaired [3]. Several researchers have noted this concern with traditional braced frames as well as BRBFs [4–7]. Moreover, recent events, such as the 2011 Christchurch Earthquake [8], have provided a reminder of how important designing beyond the traditional "life safety" level can be (e.g., using low-damage systems [9]); the social and economic impact can be significant even when "life safety" is largely achieved.

As an alternative to a BRBF (or any other elastoplastic-type system), several researchers have investigated the benefits of systems that have deliberate recentering mechanisms [10,11]. Analytical and experimental studies have shown promise in recentering system response, demonstrating that they are a viable alternative to both traditional and

* Corresponding author.
E-mail addresses: matthew.speicher@nist.gov (M.S. Speicher), reginald.desroches@ce.gatech.edu (R. DesRoches), rleon@vt.edu (R.T. Leon).
[1] Formerly Ph.D. Candidate, Georgia Institute of Technology.

http://dx.doi.org/10.1016/j.jcsr.2016.11.022
0143-974X/Published by Elsevier Ltd.

advanced systems, especially when residual deformations are of concern.

In this study an SMA-based recentering system is developed and tested (as part of a larger investigation of SMA applications [12]). This system provides both recentering and damping in a scalable arrangement. Driven by SMA's unique ability to recover strains of up to approximately 8% through a diffusionless phase transformation, the cornerstone of the bracing proposed herein is the ability to adjust the energy dissipation in a recentering hysteretic loop through the use of an AQ arrangement. SMA wire bundles are installed within the AQ and are tested alone and in parallel with C-shaped steel dampers. A schematic of the loading frame and the AQ is shown in Fig. 1. Though C-shaped dampers are used, a variety of options are available to provide paralleled damping, some of which are discussed in the next section.

To gain an understanding of the behavior of such a system, the details of the AQ are first outlined and then the experimental results from three braced frame experiments are presented. The behavior is then assessed in terms of strength, stiffness, recentering, and energy dissipation. This behavior is then used in an analytical study to demonstrate the potential benefits of the system.

2. Background

2.1. Articulated quadrilateral

As an alternative to a traditional bracing system, this study investigates a tension-only system that has the ability to dissipate energy and to recenter. Tension-only braced frames are typically not used in seismic regions due to their poor cyclic behavior [13]. However, in this work this deficiency has been addressed by inserting an articulated quadrilateral (AQ) element at the center of the bracing system, keeping the brace in tension over the entire cycle. Assuming rigid connecting elements, when one diagonal goes in tension, the opposite diagonal is also engaged in tension due to the kinematics of the AQ (i.e., for every unit expansion of the diagonal that intersects the AQ acute angle corners, the opposite diagonal has a contraction greater than that unit expansion). Therefore, the braces are continuously engaged even during load reversals. For non-rigid connecting elements, some slack is introduced in the opposite diagonal but the elements in the center of the AQ are essentially always actively engaged.

This AQ setup, pioneered by Pall and Marsh [14], has been investigated by several researchers in the past several decades in a variety of ways [15–18]. Recently, Renzi et al. [19,20] inserted C-shaped elements along the diagonal of the AQ to obtain energy dissipation. Though other options are available, in this study the authors selected the C-shaped element for the energy dissipater due to the good response reported in the literature. Collectively, the previous research has shown that tension-only AQ braces can produce stable cyclic behavior via either friction or material yielding driven by the AQ kinematics.

2.2. Recentering systems

The key characteristic of the bracing system studied in this research is its recentering ability. Recentering, as an approach to lateral load resistance, has been studied by several researchers since at least the early 1990s. Some of the first tests were a series of experiments on post-tensioned precast concrete connections [21–24]. Other researchers have expanded the idea to steel moment-resisting frames [25–27] and bracing systems [28,29].

A comprehensive study on recentering systems was conducted by Wang and Filiatrault [27]. This study consisted of shake-table testing of a three-story post-tensioned steel frame and an accompanying in-depth investigation into a single-degree-of-freedom system. Overall, the study demonstrated that good seismic performance can be reached with a recentering system. Peak story drifts were comparable to those of a traditional system (i.e., elastoplastic response) while residual drifts were essentially eliminated. However, the analysis did indicate higher maximum accelerations for the recentering system. Similar observations are noted in other single-degree-of-freedom studies [30].

Additionally, recentering systems based on allowing the frame to "rock" have gained attention in both the research and practitioner community. Several recent studies have shown the fidelity of such systems, such as work done by Eatherton et al. [31] and Roke et al. [32]. As a consequence, several rocking systems have been implemented in recent new buildings designs and existing building retrofits [33].

2.3. SMAs

SMAs have drawn considerable attention in the civil engineering community over the past two decades because of their unique stress-strain behavior. The combination of recentering and energy dissipation makes SMAs ideal for applications in earthquake-resistant design. In the 1990s the European Commission launched a research initiative, known as the MANSIDE (Memory Alloy for New Structural Isolation Devises) project, to investigate and implement SMAs into civil engineering structures [34]. From this project, several retrofit schemes were investigated and/or developed using SMA wires and bars [35–40]. Other researchers have since investigated the mechanical properties of SMAs [41,42] and their use in braced frames [43–45], beam-column connections [46–49], bridge deck restrainers [50,51], and reinforced concrete [52]. Though each of these investigations has shown varying degrees of success, limited applications have been implemented into real structures. Thus, this research seeks to explore another method of implementing

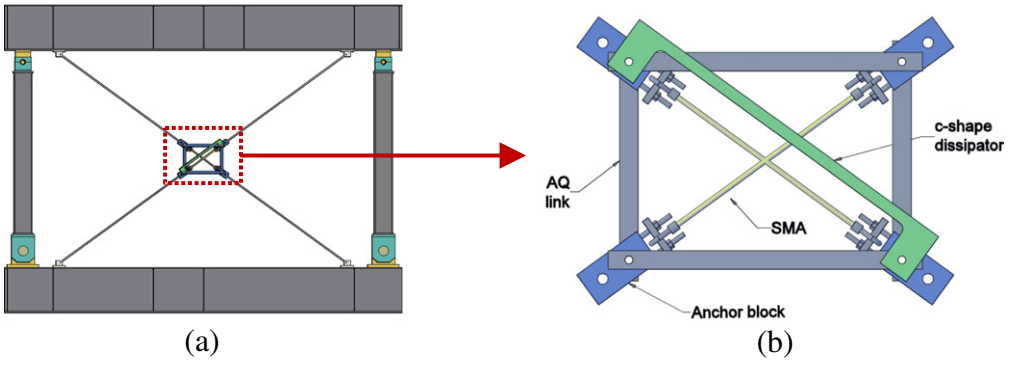

Fig. 1. (a) Loading frame schematic and (b) general articulated quadrilateral (AQ) setup with shape memory alloy (SMA) elements.

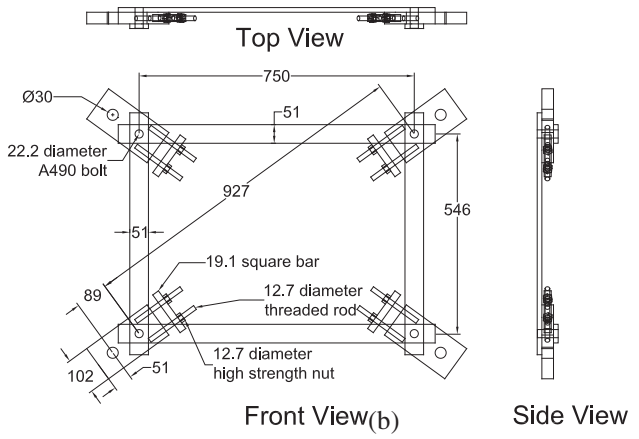

Fig. 2. Details of the articulated quadrilateral (dimensions in mm).

this unique material in which a tension-only system may be more advantageous.

3. Test setup

3.1. General setup

The general setup of the AQ is shown in Fig. 1b with both the SMA and C-shaped elements. Fig. 2 shows the resulting dimensions that were selected for the AQ. The AQ links were made from 12.7 mm thick, 50.8 mm wide A36 flat bar. The joints were pinned with 22.2 mm diameter bolts made of American Society for Testing and Materials (ASTM) A490 grade steel. The anchor blocks, made from ASTM A572 grade 50 steel, served to transfer the load from the cable assembly to the SMA wire bundles via two 12.7 mm grade 8 coarse-threaded rods connected to a 19.1 mm square bar combined with a 19.1 mm stainless steel half-round (not shown).

The dimensions of the AQ were governed by the dimensions of the loading frame (height-to-width ratio kept the same) and the length of the available SMA wire bundles. The loading frame's height and width (from the center of brace anchor points) were 4.18 m and 5.76 m, respectively. The story height was taken as 4.37 m (clear-span) for drift calculations. The SMA bundles were approximately 0.71 m long and had a cross-section of 320 individual 0.71 mm diameter superelastic NiTi wires (i.e., total cross-sectional area of 130 mm^2). To keep the SMA wires grouped together, they were wrapped in a rubber sheath. Each wire bundle was wrapped around a thimble and clamped at the ends. The effective length, defined as the distance from clamp-to-clamp, was approximately 0.56 m.

The C-shape dimensions are shown in Fig. 3. Each C-shape was fabricated from 203 mm wide, 12.7 mm thick ASTM A36 flat bar. A plasma cutter was used to cut the shape and then the edges were finished with a grinder and a mill file. Two C-shapes were combined to create the damper; one was placed on each side of the AQ face along the diagonal. The two C-shapes were tied together with clamps to prevent out-of-plane buckling (see Fig. 5). Additionally, the C-shapes had slotted holes (see Fig. 3) to allow for additional deformation capacity by relaxing the kinematic restraint that would otherwise be present. Further discussion on the development of the AQ

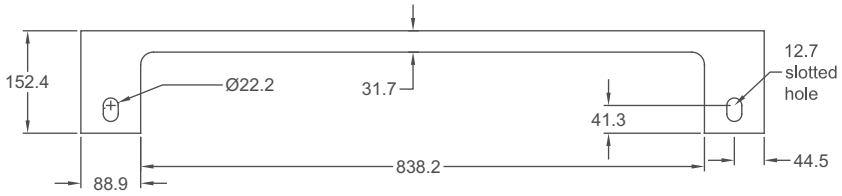

Fig. 3. C-shape dimensions (dimensions in mm).

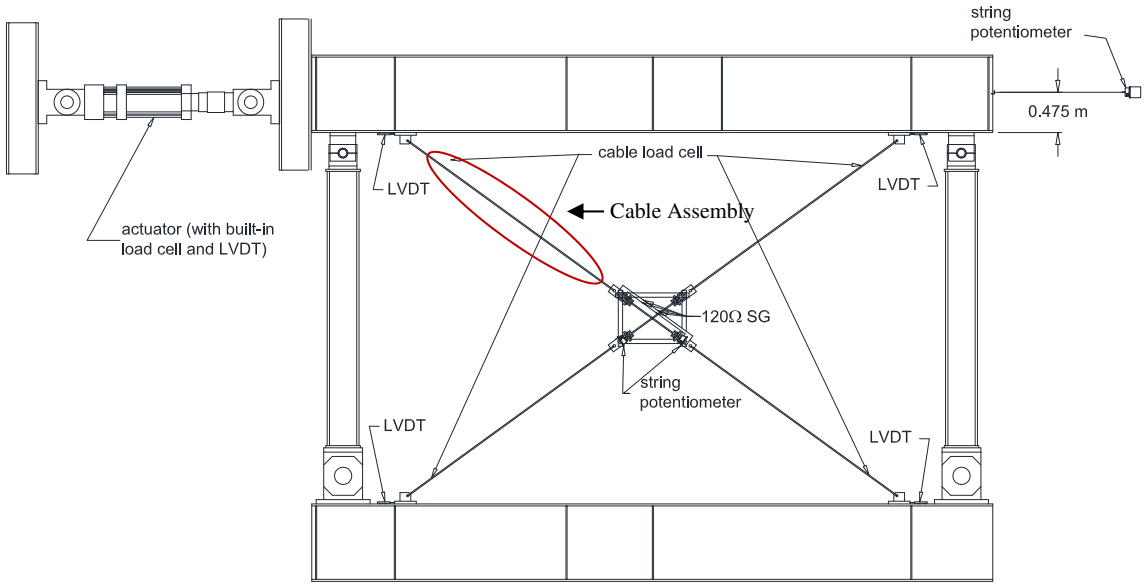

Fig. 4. Articulated quadrilateral installed in the loading frame (LVDT = linear variable differential transformer, SG = strain gage). Clear span between the loading frame beams is 4.37 m.

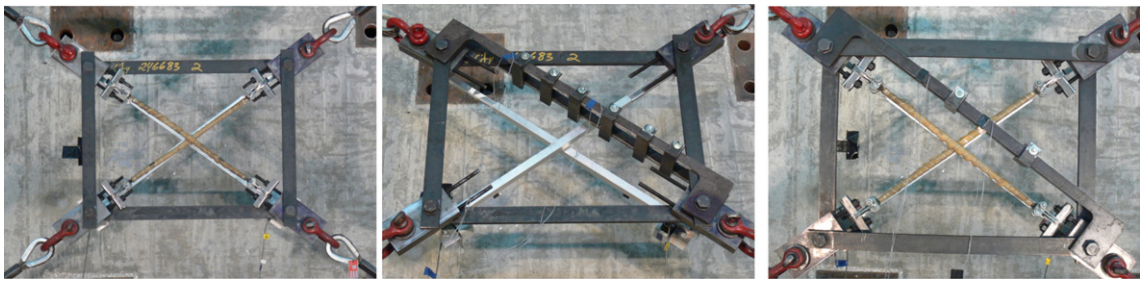

Fig. 5. Test setup for (a) the SMA only test, (b) the C-shape only test, and (c) for the parallel test. (Note: the aluminum tubes behind the AQ are used as guides for the string potentiometers).

arrangement (including the C-shaped damper characteristics) are provided in the Appendix A.

The cable assemblies that connected the AQ to the loading frame were made up of the following:

a) 25.4 mm 18–7 bright wire cable with thimbles and swag sleeves at each end
b) 25.4 mm take-up turnbuckle with jaw-jaw ends
c) 22.2 mm Crosby shackle
d) tensile load cell made from 25.4 grade 8 coarse-threaded rod
e) pad-eye anchor attached to the testing frame with four 22.2 mm A325 bolts

The entire bracing system is shown in the loading frame in Fig. 4.

The frame was instrumented to record base shear, cable forces, AQ deformations, and slippage of the cable anchor points. The story shear was captured via the actuator load cell (1000 kN capacity) and verified using the set of tensile load cells. The actuator load cell has an expanded uncertainty in the testing range of ± 3.5% (uncertainty is reported at the 95% confidence level assuming a Gaussian distribution). The cable forces were monitored via the tensile load cells installed in-line with the cables (expanded uncertainty ± 0.7% in testing range). The story drift and AQ deformations were monitored via string potentiometers (expanded uncertainty ± 0.6% in testing range). Additionally, slippage of the pad-eyes was monitored via linear variable differential transformers (LVDTs).

3.2. Testing scheme

The SMA wire bundle was first subjected to a one-sided cyclic test to determine its mechanical behavior. Next, three braced frame tests were conducted to determine the contributions of the wire bundle and the C-shaped damper to the overall behavior. The first test was with the SMA wire bundle only (*Test A*, Fig. 5a). The next test was with the C-shaped damper only (*Test B*, Fig. 5b). Six tie clamps were installed to prevent out-of-plane buckling. The final test was with the SMA and C-shaped damper in parallel (*Test C*, Fig. 5c). In *Test C*, only two tie clamps were installed on the C-shaped damper. Since C-shaped dampers are not the only damping option in such an arrangement (see Section 2), separating the behavior of the SMA wire bundle and C-shaped damper demonstrate a clearer picture of the interaction of the two components.

For each test the cables were pre-tensioned to approximately 6.7 kN. The tests were performed at a room temperature of 26 ± 1 °C. The braced frame was subjected to a cyclic loading protocol modeled after that given in the *Seismic Provisions for Structural Steel Buildings* (AISC 341–05) Appendix S [53]. In general, the loading protocol consisted of six cycles at 0.375%, 0.50%, and 0.75% drift, followed by four cycles at 1% drift, and finished with two cycles at 1.5%, 2%, and 3% drift. Higher drift levels were not induced due to stroke limitations of the actuator and load limitations on the tensile load cells.

4. Results

4.1. Mechanical test

A cyclic tension test was initially conducted on the SMA wire bundle in a conventional universal testing machine. The far-field SAC loading protocol [54] was selected for this test. The force-deformation response from the SMA wire bundle is shown in Fig. 6. The bundle demonstrated large ductility (stress plateau of approximately 5 times the transformation strain) and residual deformations less than 1% after being cycled beyond 11% gross strain. The transformation force (i.e., force at which the SMA transforms from austenite to martensite) was approximately 70 kN which corresponds to a stress of 54 MPa.

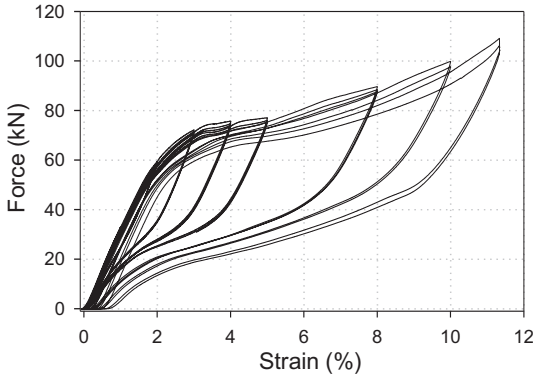

Fig. 6. Cyclic test of the SMA wire bundle with effective length taken as 5.6 m (see Test setup section for discussion on measurement uncertainty).

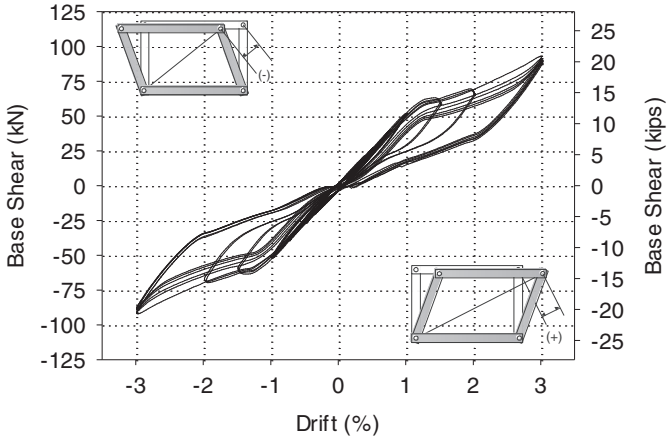

Fig. 7. Base shear versus drift for *Test A* (SMA only).

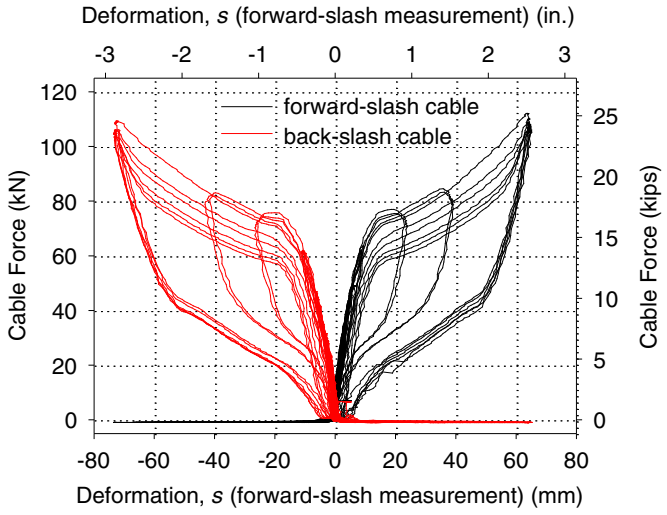

Fig. 8. Cable force versus deformation of AQ for *Test A* (SMA only).

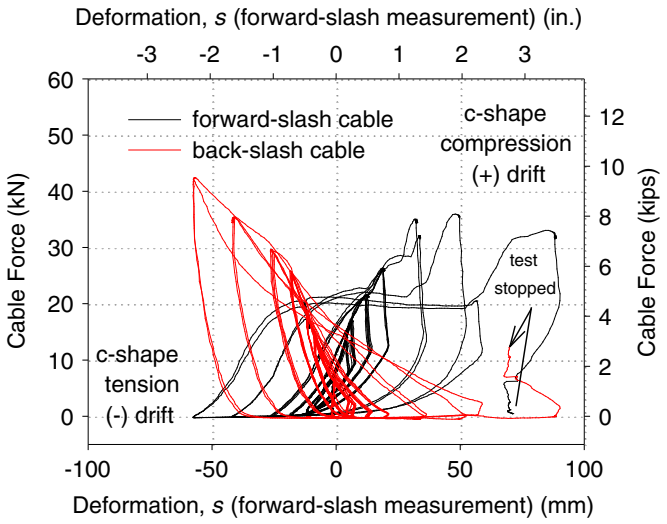

Fig. 10. Cable force versus deformation of AQ for *Test B* (C-shaped damper only).

4.2. Test A

In *Test A*, SMA wire bundles were the only elements installed in the AQ. The resulting base shear vs. story drift is shown in Fig. 7, assuming the story height to be 4.37 m. The brace remained elastic through the 1.0% drift level, with recentering to approximately 0.25% or less at the end of each cycle.

During the first 1.5% drift cycle, the SMA reached its transformation stress, as is evident by the load plateau. Fig. 8 shows the cable force (averaged from the two load cells on each diagonal) versus the AQ deformation. This figure shows essentially the force-deformation plot of the SMA elements, with the forward-slash (bottom-left to top-right measurement) and back-slash (top-left to bottom-right measurement) cables being engaged in opposing directions.

During the 2% drift cycle, the SMA was stretched further along its loading plateau but not completely into its martensitic phase. The brace showed minimal strength degradation and minimal stiffness degradation. To finish the test, the frame was cycled six times at 3% drift. The brace began to display strength degradation and began to accumulate residual deformations (and therefore effective-stiffness degradation). However, the response stabilized after about four cycles. The strength degradation in the first few loading cycles of shape memory alloys is a well-known phenomenon that can be reduced through cycling of the material [39,40].

4.3. Test B

In *Test B*, two C-shaped dampers were installed in the AQ. The resulting base shear versus story drift is shown in Fig. 9. The brace remained essentially elastic through the 0.5% drift cycles, with only small hysteretic loops forming. During the 0.75% and 1.0% cycles, the hysteresis area increased, indicating the C-shaped dampers were being deformed beyond their elastic limit. Fig. 10 shows the measured cable force versus AQ deformation. This plot is similar to the force-deformation plot of the C-shaped damper. During the 1.5% drift cycles (and beyond), the clamps that connected the two C-shapes together began bearing against the AQ links. This resulted in a jump in stiffness upon further loading and eventual flexural yielding of the AQ links. This issue was corrected in *Test C* by adding fewer tie clamps while still maintaining out-of-plane stability of the C-shaped damper.

At larger drift levels, the brace stiffened when cycled to the left (negative drift). This response was caused by the tension/compression asymmetry of the C-shaped damper which was the result of the deformation transitioning from flexural rotation to axial stretching. To alleviate some of the stiffening, slotted holes were introduced for *Test C*. Nevertheless, the brace strength and stiffness were stable and the C-shaped damper was able to deliver hysteretic damping. The test was stopped after the first 3% cycle due to flexural yielding of one of the AQ links caused by bearing of the C-shaped damper ties.

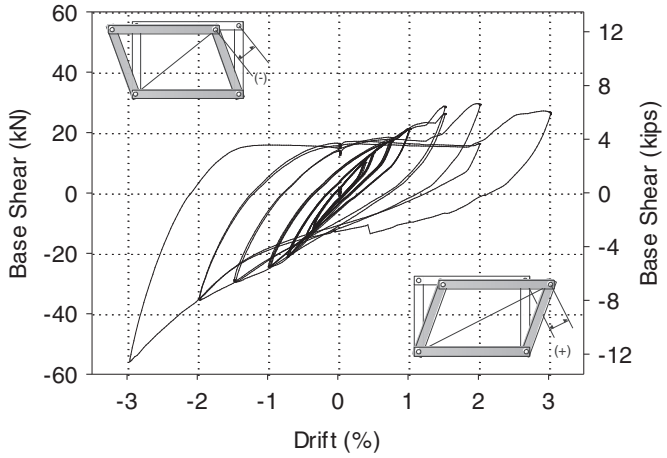

Fig. 9. Base shear versus drift for *Test B* (C-shape only).

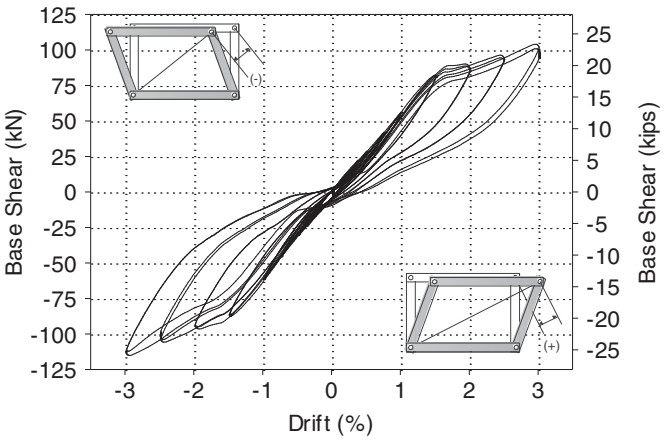

Fig. 11. Base shear versus drift for *Test C* (PARA).

4.4. Test C

In *Test C*, two C-shaped dampers were combined in parallel with SMA wire bundles. The resulting base shear versus story drift is shown in Fig. 11. The brace remained mostly elastic through the 1.5% drift cycles, with recentering to approximately 0.15% at the end of each cycle.

During the 2.0% cycle, the SMA elements reached their transformation stress, as is evident by the load plateau in Fig. 11. Fig. 12 plots the cable force versus the AQ deformation. This plot is similar to the force-deformation plot of the SMA elements paralleled with the C-shaped dampers.

During the 2.5% drift cycle (added for this test), the SMA was pushed further along its loading plateau. The brace showed little strength and stiffness degradation. To finish the test, the frame was cycled twice at 3% drift and the resulting deformed shape is shown in Fig. 13. As expected, the brace began to display some strength degradation and began to accumulate some residual deformations (and therefore stiffness degradation). The increased damping of the parallel system was evident in the hysteresis. Each of these observations are quantified and discussed in the next section.

5. Discussion of results

The three braced frame tests demonstrated, in a progressive manner, how the recentering inherent in SMAs can be combined with energy dissipating elements to produce a larger flag-shaped hysteresis. To assess the behavior of the braced frame, a brief discussion is first given on the general behavior of the bracing system. Next, changes over the cyclic protocol in the following four response parameters are investigated: stiffness, strength, energy dissipation, and recentering. These four response parameters are only presented for the two tests that included the SMA elements: *Test A* and *Test C*.

5.1. General behavior

Before the response parameters are examined, the effect of the relative stiffness of the elements combined to make the bracing system should be discussed. When SMA and elastic elements are combined in series, a resulting force-deformation relationship will form as shown qualitatively in Fig. 14. If the "elastic" element is rigid, the resulting series behavior would be exactly that of the SMA. However, if the "elastic" element is not rigid, the length of the loading plateau relative to the yield deformation (defined here-in as the plateau ductility factor, η) will decrease. For the series system, the plateau ductility factor is calculated by the following formula:

$$\eta = \frac{\beta + \Delta F/k_e}{u_{y,series}} \tag{1}$$

where $u_{y,series}$ is the "yield" deformation of the series system and β, ΔF, and k_e are defined in Fig. 14. To illustrate the combined effects, Fig. 15 shows the contributing elements and the series system for *Tests A*. Note that the *effective* ductility of the "series" response is less than that of the "SMA" response.

To maximize η, the brace elements combined in series with the SMA element should be sufficiently stiff. For a perfectly rigid connecting member, a η greater than four can be obtained (dependent on the SMA). For this experimental setup, η was found to be approximately 2.5, which resulted in less ductility for a given stiffness. Though this effect is noted, it is not investigated further in this study. Additional investigation needs to be performed to understand the implications of this behavior.

5.2. Stiffness and strength

Stiffness and strength are presented in terms of effective stiffness, k_{eff}, and yield base shear, V_{by}, as defined by the straight-line approximations shown in Fig. 16. The k_{eff} and V_{by} values are found to have an expanded uncertainty of approximately $\pm 1.2\%$. For the strength, "yield" corresponds to onset of the SMA phase transformation plateau. The resulting trends for stiffness and strength are plotted in Figs. 17 and 18, respectively. The stiffness generally decreased with increasing drift level, though the decrease was only 15% to 20% at 3% drift. Additionally, the "series effect" reduced the resulting stiffness of the brace. Braces in typical concentrically braced frames are expected to yield and buckle at story drifts of about 0.3% to 0.5% [53], while this brace "yielded" at 1% to 1.5% drift, which is more in line with drift levels expected in moment frames.

The strength decreased moderately during cycling for both tests. However, *Test C* decreased at a faster rate due to more residual accumulation. Additionally, *Test C* had larger stiffness and strength than that of *Test A* due to the addition of the C-shaped dampers. As noted in Fig. 18, the "yield" base shear was reached at different drift levels due to the adjoining cable assembly's elastic deformations. It is anticipated that the system's effective stiffness before "yield" could be increased by increasing the pretension in the cable assemblies, which would correspondingly decrease the system's "yield" drift. Nonetheless, after the braces begin to deform, the system's instantaneous stiffness would not change until the onset of the SMA phase transformation or other nonlinear phenomenon in the brace assembly.

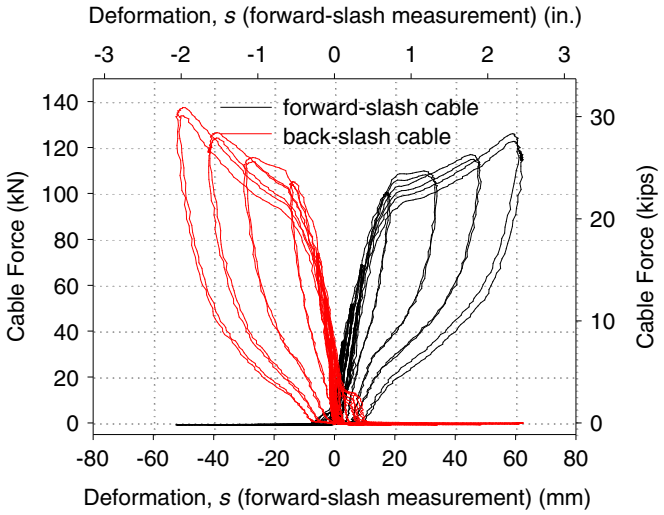

Fig. 12. Cable force versus deformation of AQ for *Test C* (PARA).

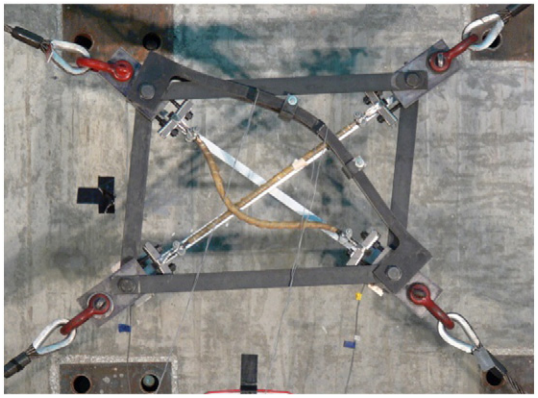

Fig. 13. Deformed shape of the AQ for *Test C* at 3% drift.

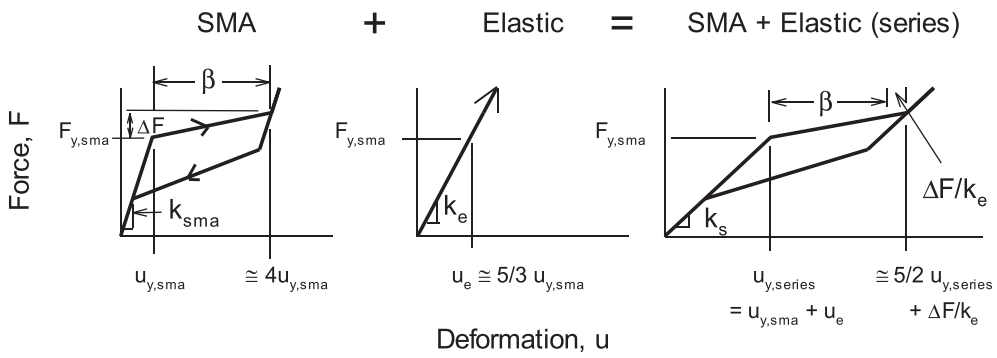

Fig. 14. Schematic illustrating the qualitative force-deformation characteristics of an SMA element combined in series with an elastic element normalized to the yield force, F_y, and yield displacement, u_y (additional definitions: β = SMA horizontal plateau length; ΔF = change in force over the SMA plateau; k_{sma}, k_e, and k_s = stiffness of the SMA element, elastic element, and series element, respectively).

5.3. Energy dissipation

Energy dissipation is reported in terms of equivalent viscous damping, ζ, defined as [55]:

$$\zeta = \frac{E_D}{4\pi E_{so}} \tag{2}$$

where E_D is the energy dissipated in one cycle and E_{so} is the energy absorbed by an equivalent linear system loaded to the same maximum force and displacement level as used in E_D. The energy dissipation (i.e., the area of the hysteresis loop) is assessed for the first and second cycles of *Tests A* and *C* and is show in Fig. 19. The expanded uncertainty was approximately ±5% of the values shown in Fig. 19. The ζ varied from 3% to 9%, with the first cycle's damping generally greater than that of the second cycle. At 0.375% and 0.5% drift, the ζ was greatly influenced by the friction in the system. Friction had less of an effect at the 1.0% drift level, therefore the damping dropped. However, at drifts greater than 1.0%, the ζ for both tests increased rapidly due to the SMA being pulled into its transformation range.

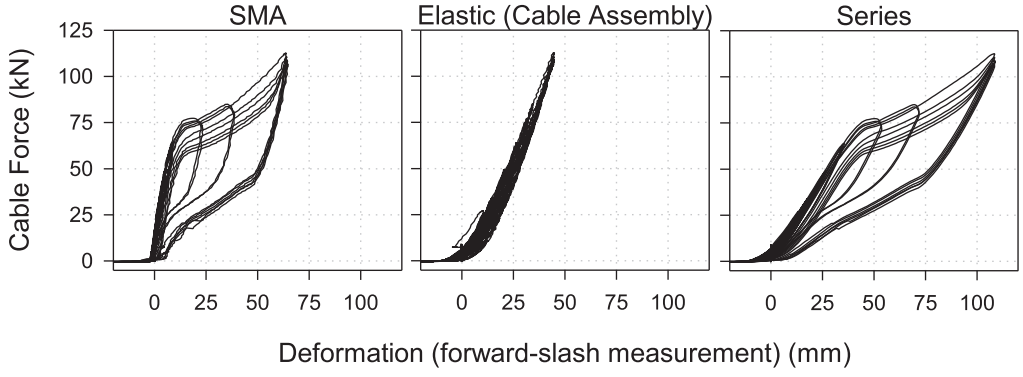

Fig. 15. Contributions of the different brace elements in series for *Test A*.

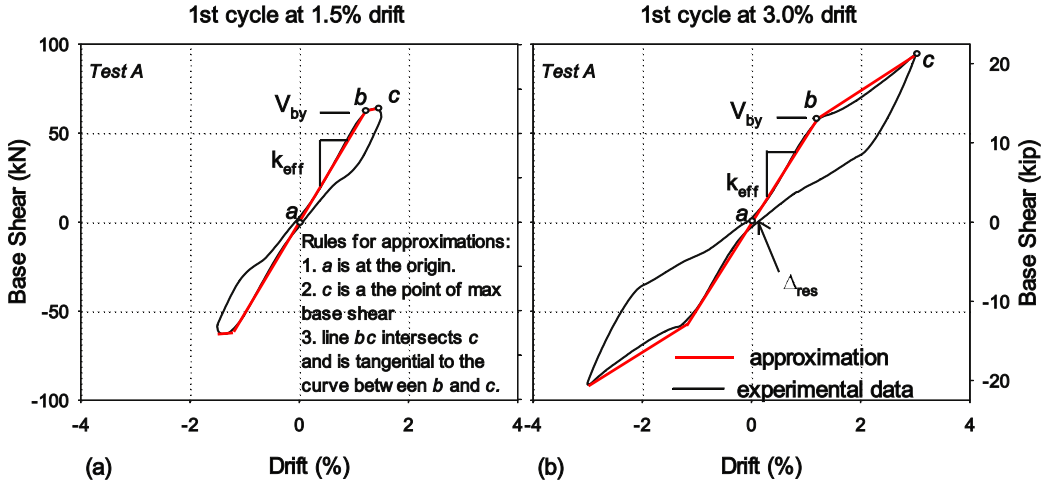

Fig. 16. Straight-line approximations of the base shear versus drift response to obtain the "yield" base shear, V_{by}, and the effective stiffness, k_{eff}.

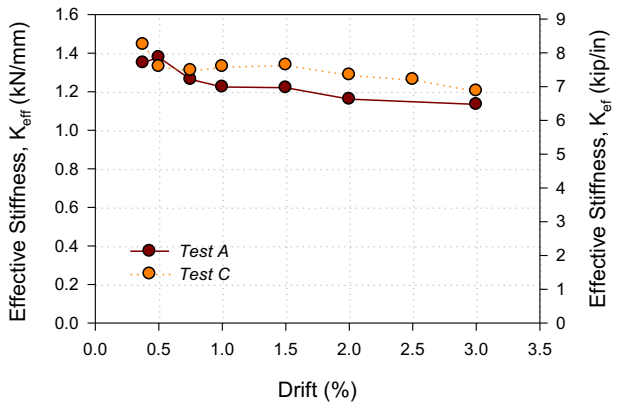

Fig. 17. Effective stiffness, K_{eff}, over a range of drift levels for *Tests A* and *C*.

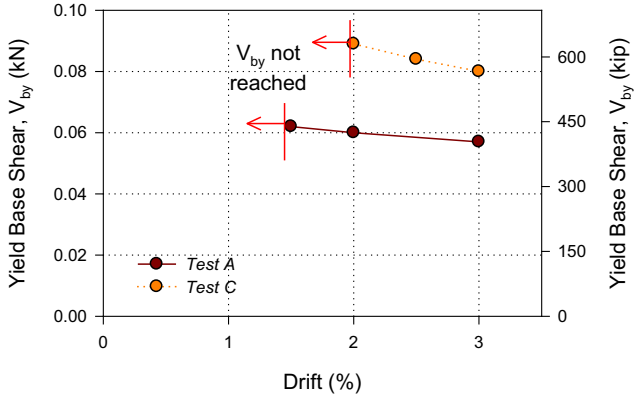

Fig. 18. "Yield" base shear, V_{by}, over a range of drift levels for *Tests A* and *C*.

For 1.5% to 3% drift, the ζ was approximately 6% to 8% for *Test A* due to the hysteresis that formed in the SMA wires. For *Test C*, the ζ did not increase as quickly because a higher drift level was needed to force the SMAs into its phase transformation. This behavior was due to the increased stiffness in the AQ elements which resulted in the cable assemblies having increased deformations. For 2% to 3% drift, the ζ was approximately 7% to 9% for *Test C*.

Though recentering is the main focus of this bracing system, added damping can have a positive impact on a recentering system's performance [30]. The purpose of adding the C-shaped damper in parallel with the SMA wire bundle was to enhance the brace's energy dissipation. In this regard, the ζ plots are slightly deceiving because the two systems have different "yield" drifts and "yield" strengths. This effectively shifted the response of *Test C*'s ζ to the right by approximately 0.5% drift. With this in mind, the damping of *Test C* was enhanced by the addition of the C-shaped damper, as would be expected.

5.4. Recentering

Recentering is assessed by looking at the residual drift (Δ_{res}) defined as the point at which the force versus deformation curve crosses the zero force level during each cycle. The residual drifts over the cycle histories are shown in Fig. 20; the expanded uncertainty in the reported residual drift values is approximately ± 1.0%. *Test A* exhibited the most effective recentering behavior, having only 0.12% residual drift after the frame had been subjected to 3.0% drift. *Test C* had approximately four times more residual drift than *Test A* due to the C-shaped damper preventing full recentering. Although not done in this study, improved recentering behavior could likely be obtained by increasing the pretension in the SMA wire bundles.

6. Analytical study

6.1. Model

To further investigate the effectiveness of the SMA-based bracing system, the response of a seven-story building outlined in the 2005 NEHRP Design Examples (FEMA 451, Section 5.2, Alternative B [56]) is investigated. The building layout and member sizes are not reproduced here but are available in [56].

The building was modeled using the OpenSees [57] structural analysis software. To simplify the analysis, only one direction of loading was considered (North-South) and only one braced-frame bay was modeled. Since the building was designed with four braces in the North-South direction, one-fourth of the mass was lumped at each floor height (half at each intersecting beam-column node). The lateral resistance of the non-braced frames was ignored and torsion was not considered. The columns were fixed at the base and the beam-column connections were pinned, thus neglecting the gusset plate stiffness.

Four different brace behaviors were investigated as shown in Fig. 21. The stiffness and yield strength of all the braces were considered equal. The special concentrically braced frame (SCBF) (*Brace A*) was calibrated to buckle in compression at the design nominal capacity, P_n, and have a post-buckling strength of $0.3P_n$ at 20 times the buckling deformation using initial out-of-straightness and end rotational springs. The SMA brace (*Brace B*) was created using a one-dimensional constitutive model first proposed by Auricchio and Sacco [58] and later modified and implemented into OpenSees by Fugazza [59] (note: at the time this paper was written, this model no longer exists in the current version of OpenSees). The brace made of the SMA and C-shaped damper in parallel (PARA; *Brace C*) was created using a parallel element that

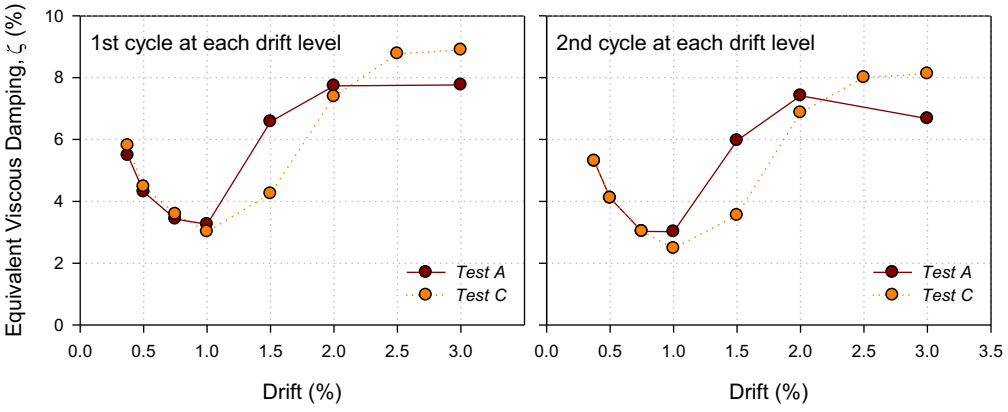

Fig. 19. Equivalent viscous damping in the first and second cycle for *Tests A* and *C*.

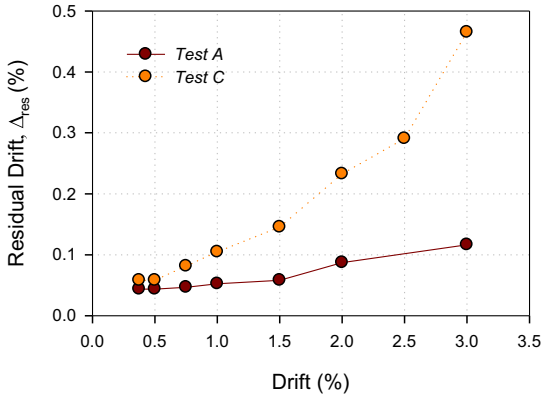

Fig. 20. Residual drift (Δ_{res}) over a range of drift levels in *Tests A* and *C*.

combined the behavior of SMAs with that of the *Steel01* (elastoplastic with strain hardening) material model. The area of the parallel element was made up of 80% SMA and 20% elastoplastic behavior derived from the experimental results. The buckling-restrained braced frame (BRBF; *Brace D*) was a simplified representation of a buckling-restrained brace response created with the *Steel01* material model. Engineering judgement was used when determining the force-deformation responses without considering refinement of the design parameters (i.e. R, C_d, and Ω_0 factors). This refinement could be the subject of further investigation.

The braced frame was subjected to a suite of ground motions from the Los Angeles, California region (LA21 to LA40) with a 2% probability of exceedance in 50 years taken from Somerville et al. [60]. No scaling was applied to the ground motions.

6.2. Results and discussion

To illustrate the behavior of the four brace types, the base shear versus first story drift in response to the LA25 ground motion is shown in Fig. 22a–d and the first story drift response history is shown in Fig. 22e. The maximum first story drifts for *Braces A to D* were 3.2%, 1.6%, 1.6%, and 2.3%, respectively. The residual first story drifts for *Braces A* and *D* were 1.3% and 0.7%, respectively. Notably, *Braces B* and *C* showed no residual drifts for this ground motion. Both systems with SMA had approximately 50% reduction in the maximum drift amplitude compared to the SCBF and a 30% reduction compared to the BRBF. Furthermore, the SCBF and the BRBF both exhibited significant residual drift, as opposed to the SMA-based systems.

However, the results from the LA25 ground motion must be reviewed with caution. The force levels in both SMA systems reached up into the post-plateau stiffness region. From mechanical tests, it is apparent that SMAs begin to lose their superelasticity (and thus accumulate residual strains) in this region, which was not captured in the analyses. Additionally, higher forces in these elements could be problematic due to overloading of other elements. Further analysis is recommended to determine appropriate design procedures to mitigate these issues.

With respect to the entire suite of ground motions, the response of each braced frame is summarized in Fig. 23. The following observations are made:

- The SCBF had large drifts forming in the first, second, and third stories. Drifts exceeded 3% in the second story for several ground motions, which may result in collapse of the building. However, collapse is not directly accounted for in the model.
- The SMA and PARA frames were both effective in decreasing the drift demands in the first three stories. However, as mentioned above, care must be exercised in designing an SMA-based system to ensure the load plateau is not being exceeded, otherwise forces being transferred to adjacent members could violate the capacity design philosophy and result in yielding in other elements of the structure.
- The SMA and PARA frames had smaller maximum interstory drifts compared to the SCBF and the BRBF. This was due to the SMA and PARA frames' ability to distribute the drift demand more uniformly along the height of the structure.
- In comparing the SMA and the PARA frames, the PARA system had a slight performance advantage in terms of maximum drifts. However, the results are not conclusive. Further investigation needs to be conducted to more fully understand the impact of a PARA system on the response of a complete structural system.
- The residual drifts were greatest in the SCBF, where the bottom three stories had an average residual drift of 0.6%. The BRBF was also prone to accumulating residual drifts, though, on average, the residual drifts were approximately half those seen in the SCBF.

From these observations, the SMA-based braced frames were effective in decreasing interstory drifts, did a good job of distributing the drift demands over the height of the building, and significantly reduced residual drifts.

Though the performance of this AQ system is promising, one practical challenge is the issue of scalability. The SMA wire bundle used in these tests had a cross-sectional area of 130 mm^2. This area could be increased by using larger thimbles and more wire loops or by using several wire bundles in parallel. Additionally, rather than designing a system to have the equivalent stiffness and strength as a traditional braced frame, it may be more advantageous to take advantage of the SMA's smaller elastic modulus. This reduced stiffness would facilitate a more flexible system which would increase a structures fundamental period and reduce the accompanying strength demand.

7. Summary and conclusions

In this study, an articulated quadrilateral bracing system was developed and experimentally tested as a way to leverage the beneficial characteristics of SMAs in the seismic load-resisting system of a building. The articulated quadrilateral geometry allowed the shape memory

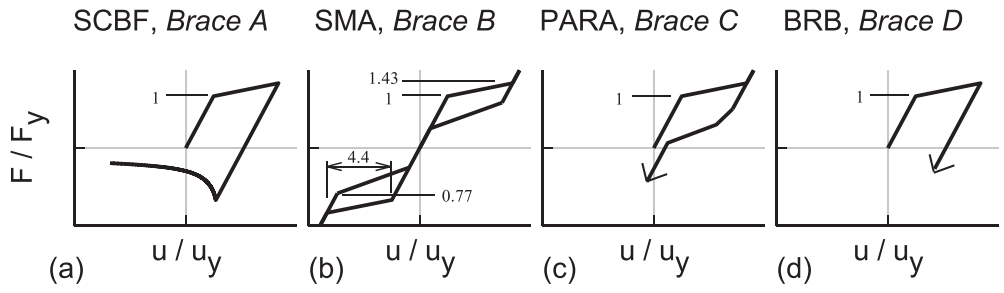

Fig. 21. Brace models used for the analyses (F/F_y = the axial force normalized by the yield force, u/u_y = the deformation normalized by the yield deformation).

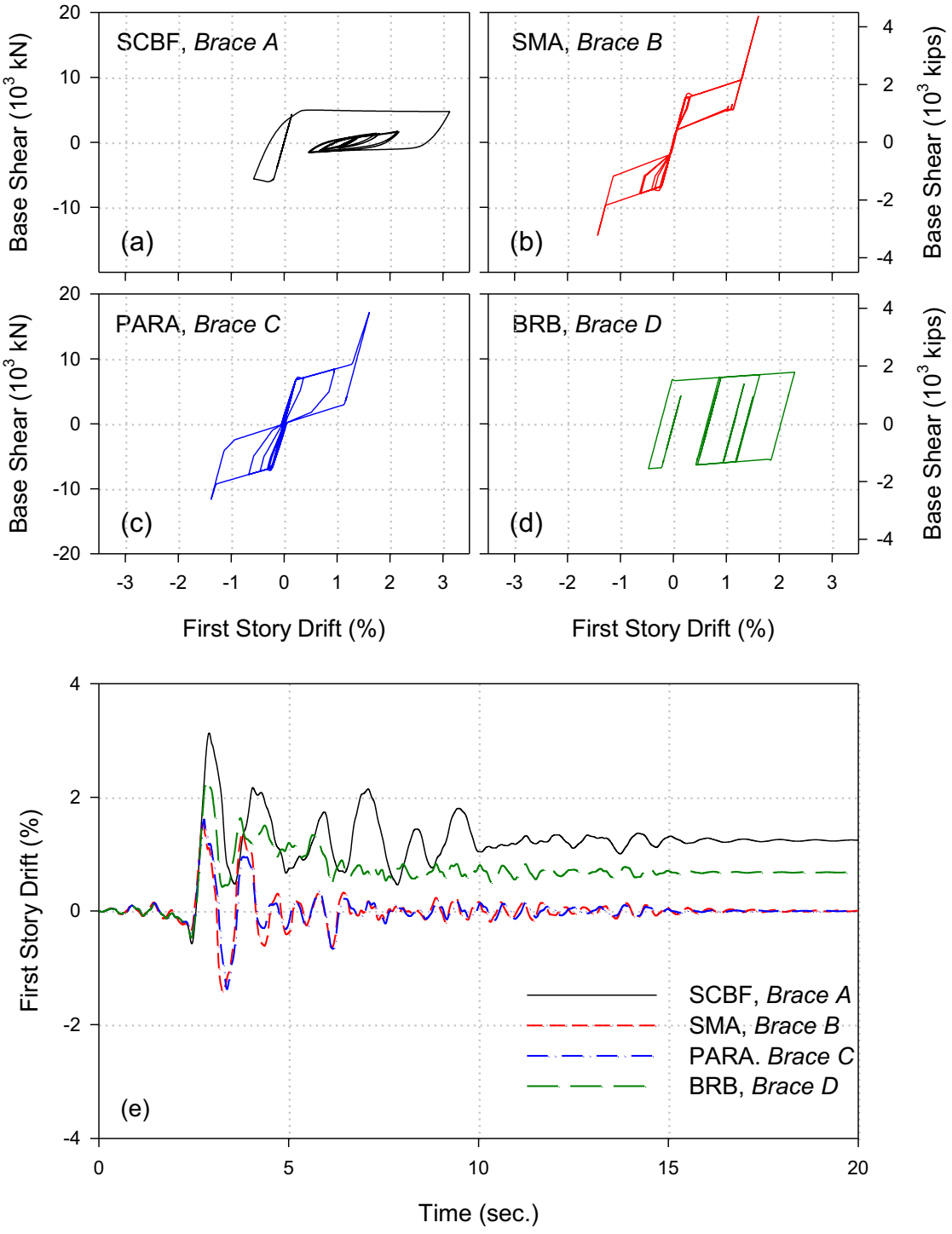

Fig. 22. (a-d) Base Shear versus first story drift and (e) first story drift response history for SCBF, SMA, PARA, and BRBF subjected to the LA25 ground motion.

alloy to be combined in parallel with an energy dissipating element. If properly calibrated, it was envisioned that this bracing system can provide building recentering with optimized energy dissipation. The following observations and conclusions are made from this investigation:

- SMA wire bundles were able to recover large levels of gross strain (11%).
- The relative stiffnesses of the elements combined to make the bracing assembly influence the length of the load plateau relative to the yield deformation, i.e. plateau ductility factor. To maximize this factor, which is desirable for robust seismic performance, the brace elements combined in series with the SMA element must be sufficiently stiff to fully utilize the beneficial properties of the SMA. In our experiments, the brace had a plateau ductility factor of approximately 2.5.
- The C-shaped damper displayed stable hysteretic behavior and can be fabricated to a variety of strength, stiffness, and deformation capacities.

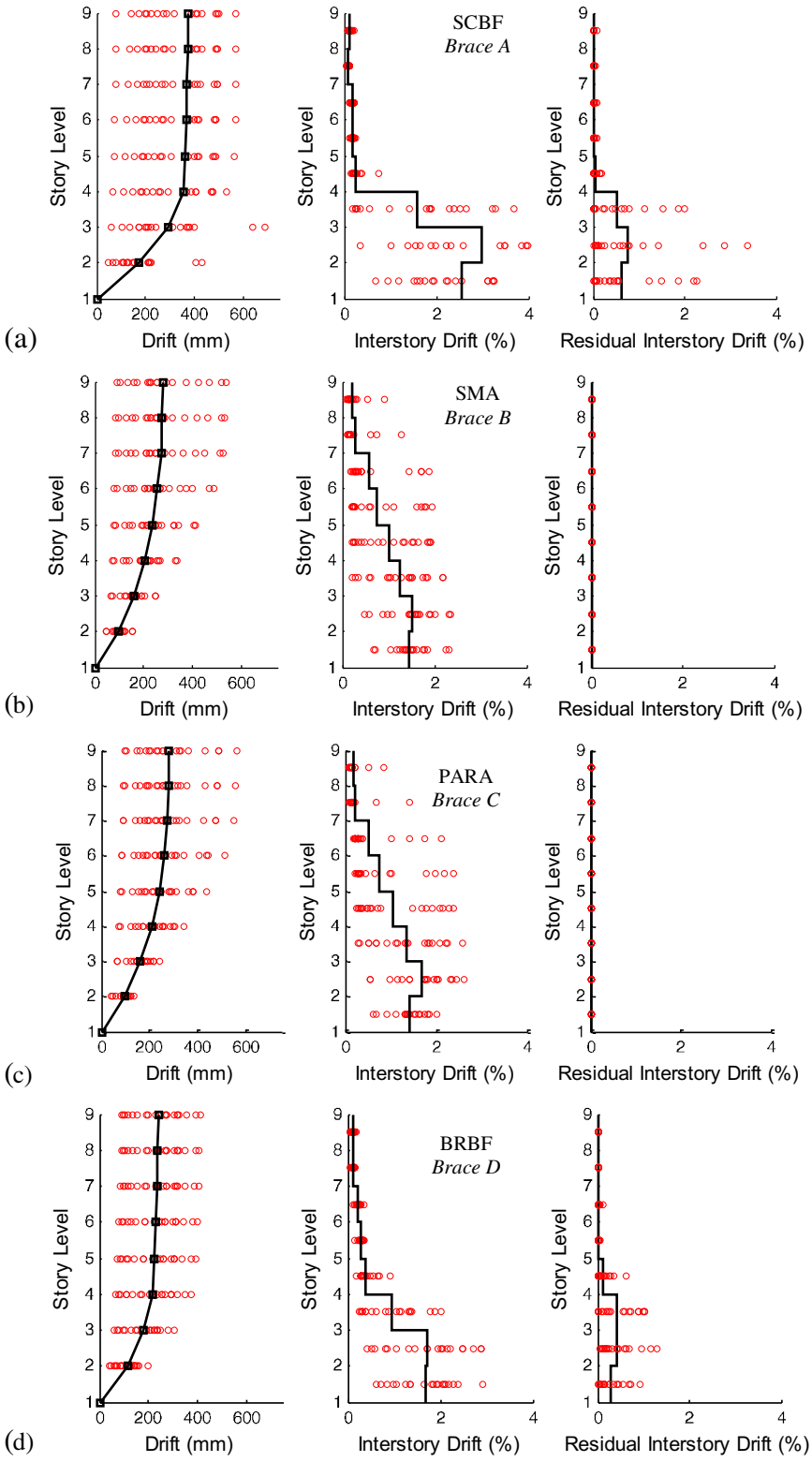

Fig. 23. Drift, interstory drift, and residual drift in response to the investigated ground motions for the first story of the (a) SCBF, (b) SMA, (c) PARA, and (d) BRBF. Braces *A-D* (mean = black line, data = red circles).

- The SMA-only bracing system was the best choice when residual drifts needed to be minimized. The frame had residual drifts of less than 0.1% after being pushed to 3% story drift.
- The combined SMA and C-shaped damper bracing system (PARA) displayed increased damping. However, full recentering was sacrificed to obtain this additional damping. The frame had residual drifts of 0.5% after being pushed to 3% drift.
- Both SMA-only and the PARA systems had minimal loss in strength and stiffness after repeated cycling.
- From the analysis of a seven story building subjected to twenty far-

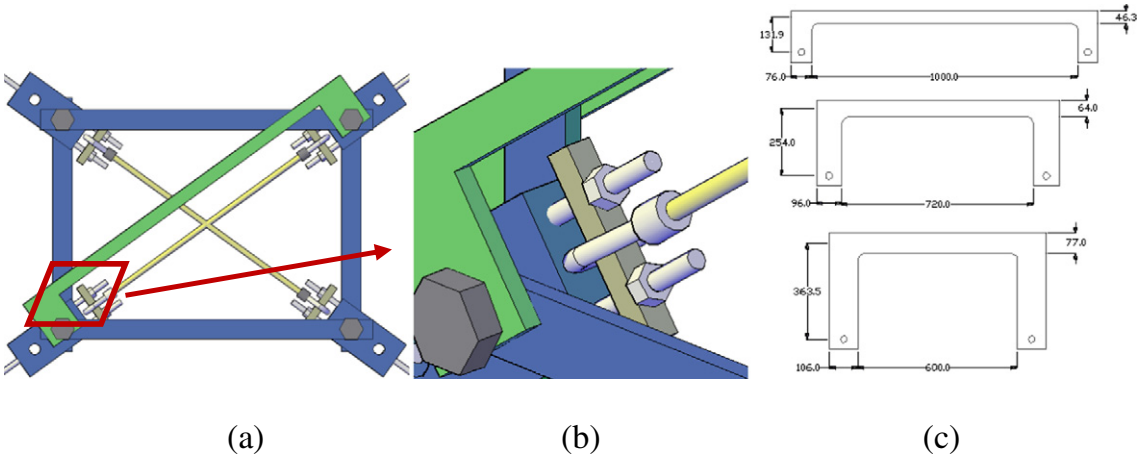

Fig. 24. (a) Articulated quadrilateral with SMA bundles and C-shape dissipaters, (b) 3D view of SMA attachment, and (c) C-shape dimension variation for constant thickness, stiffness, and yield force.

field ground motions, the SMA and PARA systems had the best performance in terms of interstory and residual drifts. These systems both tended to distribute the drifts more evenly over the height of the structure, thus reducing the likelihood of the formation of a soft-story.

This investigation was exploratory in nature, focusing on the effects of recentering vs. energy dissipation, and the feasibility of using shape memory alloys in conjunction with damping materials. It is recommended that further work be done to refine the articulated quadrilateral device and more fully determine the performance advantages and limitations. Some areas of future work could include the following: varying the amount of pretension in the articulated quadrilateral and the adjoining cable assembly, investigating other methods of adding damping, and investigating the ability of such a system to handle full-scale loads.

Disclaimer

Certain software may have been used in the preparation of information contributing to this paper. Identification in this paper is not intended to imply recommendation or endorsement by the National Institute of Standards and Technology, nor is it intended to imply that such software is necessarily the best available for the purpose.

Acknowledgements

The authors would like to thank Dr. Darel Hodgson of Nitinol Technology Inc. for his contributions in the development and fabrications of the SMA wire bundles.

Appendix A

One of the main goals of this bracing system was to create an effective way to combine SMA elements in parallel with supplemental energy dissipating elements. This idea was rooted in the following result observed in previous work [30]: a recentering system with a maximized hysteretic loop will produce the best performance. To dissipate energy by yielding or by friction, the dissipating element must be subjected to load reversal (i.e., tension and compression). For a cable bracing system, this is difficult to obtain without a special arrangement. The AQ configuration accomplishes this requirement in a unique way and facilitates the use of a variety of dissipating elements.

Several options for dissipating elements have been identified including torsional dissipators (either friction or yielding) at the AQ joints,

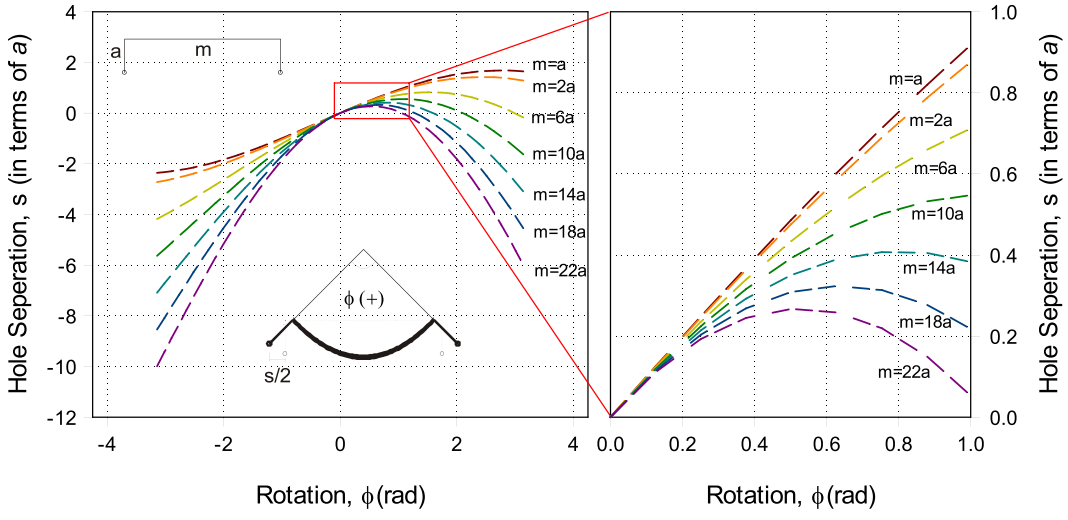

Fig. 25. C-shape kinematic behavior assuming the center of C-shape is axially inextensible and the arms are completely rigid.

frictional dissipaters on the diagonals [14], flexural yielding of the AQ members [17], and C-shaped dissipators on the diagonals [19]. The C-shaped damper was chosen for this research because of the predictable results shown in experimental work by Renzi [19]. Nevertheless, the other methods of providing energy dissipation should not be discounted and have been found to be very successful in research and application.

The options for loading the SMA elements include torsion at the joints and tension across the diagonal. The latter option was chosen because tension is the most efficient use of the material. Additionally, superelastic NiTi wires have been shown to have excellent performance in terms of inherent energy dissipation and recentering. A bundle of NiTi wires was fabricated by Nitinol Technologies Inc. The full details of the NiTi bundles are described in the component test section of this paper.

Fig. 24(a) and (b) shows a schematic of the complete AQ setup. The SMA bundles cross in the middle and are anchored to square steel bars at the ends. This steel bar is then mounted to threaded bars which are inserted into a steel transfer block. This setup enables tightening of the SMA bundles to either remove slack or to instill some initial pretension while maintain a configuration that is as compact as possible. The C-shaped damper members are attached at the corner joints with a large diameter bolt functioning as a pin. Two C-shaped dissipators were used in the same direction but on opposite faces of the AQ. Due to the geometry implemented, out-of-plane ties were attached to the C-shaped damper along the length. These ties effectively braced the two dissipators together and forced flexure yielding to occur before lateral torsional buckling.

The dimensions and the material properties of the C-shape determined its strength and stiffness. When selecting the dimensions, the following criteria were adhered to:

- The thickness of the C-shape should be minimized to ensure the AQ's compactness (12.7 mm was selected in this study).
- The yield strength should be the fraction of the SMA element yield that creates increased system damping while maintaining good recentering. The yield strength was selected to be 22 kN, the approximate end of the unloading plateau seen in mechanical testing of the SMA wire bundle.
- The stiffness of the C-shape should be greater than or equal to the stiffness that results in the C-shape yielding at the same deformation as the SMA. This criterion ensures the C-shape is pushed beyond its elastic range.

To show the effects of length change, Fig. 24c provides a graphical illustration of how the dimensions of a C-shape change when thickness, stiffness, and yield force are held constant and length is varied.

For this research, the length is predetermined by the length of the SMA wire bundles. Because of the length, strength, and stiffness requirements, the C-shape is long. In Fig. 25 the relationship between hole separation, s, and arm rotation, f, is plotted for a range of m/a ratios (defined on the plot) and the governing equation is:

$$s = 2\left(a + \frac{m}{\varphi}\right)\sin\left(\frac{\varphi}{2}\right) - m \qquad (a.1)$$

This equation and corresponding plot assume that the C-shape body (m portion) is axially inextensible and that arms (a portions) are rigid. The maximum hole separation for each m/a gives the limitation of each C-shape geometry. If further hole separation is induced, the deformation mode will be axial extension rather than flexural bending. Slotted holes were implemented in the experimental specimen to work around this constraint.

References

[1] S.A. Mahin, Lessons from damage to steel buildings during the Northridge earthquake, Eng. Struct. 20 (1998) 261–270.

[2] AISC, Seismic Design Manual, Third Printing ed. American Institute of Steel Construction, 2006.

[3] C.M. Ramirez, E. Miranda, Significance of residual drifts in building earthquake loss estimation, Earthq. Eng. Struct. Dyn. 41 (2012) 1477–1493.

[4] S. Kiggins, C.-M. Uang, Reducing residual drift of buckling-restrained braced frames as a dual system, Eng. Struct. 28 (2006) 1525–1532.

[5] R. Sabelli, S. Mahin, C. Chang, Seismic demands on steel braced frame buildings with Buckling-restrained braces, Eng. Struct. (2003).

[6] J. Erochko, C. Christopoulos, R. Tremblay, H. Choi, Residual drift response of SMRFs and BRB frames in steel buildings designed according to ASCE 7-05, J. Struct. Eng. 137 (2011) 589–599.

[7] L.A. Fahnestock, J.M. Ricles, R. Sause, Experimental evaluation of a large-scale buckling-restrained braced frame, J. Struct. Eng. 133 (2007) 1205–1214.

[8] C. Clifton, M. Bruneau, G. MacRae, R. Leon, A. Fussell, Steel structures damage from the Christchurch earthquake series of 2010 and 2011, Bull. N. Z. Soc. Earthq. Eng. 44 (2011) 297–318.

[9] S. Pampanin, Reality-check and renewed challenges in earthquake engineering: implementing low-damage systems - from theory to practice, Bull. N. Z. Soc. Earthq. Eng. 45 (2012) 137–160.

[10] M.M. Garlock, R. Sause, J.M. Ricles, Behavior and design of posttensioned steel frame systems, J. Struct. Eng. 133 (2007) 389–399.

[11] M.R. Eatherton, M. Xiang, H. Krawinkler, G.G. Deierlein, J.F. Hajjar, Quasi-static cyclic behavior of controlled rocking steel frames, J. Struct. Eng. 140 (2014), 04014083. (11 pp.).

[12] M. Speicher, Testing and Assessment of SMA-Based Recentering Systems, Georgia Insitute of Technology, Atlanta, GA, 2009.

[13] M. Bruneau, C.-M. Uang, A.S. Whittaker, Ductile Design of Steel Structures, McGraw-Hill, New York, 1998.

[14] A.S. Pall, C. Marsh, Response of friction damped braced frames, J. Struct. Div. ASCE 108 (1982) 1313–1323.

[15] R.G. Tyler, Further notes on a steel energy-absorbing element for braced frameworks, Bull. N. Z. Soc. Earthq. Eng., 18, 1985, pp. 270–279.

[16] R.G. Tyler, Test on a brake lining damper for structures, Bull. N. Z. Soc. Earthq. Eng., 18, 1985, pp. 280–288.

[17] R.G. Tyler, Preliminary tests on an energy absorbing element for braced structures under earthquake loading, Bull. N. Z. Soc. Earthq. Eng., 16, 1983, pp. 201–212.

[18] V. Ciampi, M. Arcangeli, S. Perno, Characterization of the low-cycle fatigue life of a class of energy dissipating devices, published in the Proceedings of the 2nd European Conference on Structural Dynamics: EURODYN '93, Trondheim, Norway, A.A. Balkema, Rotterdam, Neth 1993, p. 137 (Publ by).

[19] E. Renzi, S. Perno, S. Pantanella, V. Ciampi, Design, test and analysis of a light-weight dissipative bracing system for seismic protection of structures, Earthq. Eng. Struct. Dyn. 36 (2007) 519–539.

[20] E. Renzi, N. Ranieri, G. DeCanio, Experimental verifications of seismic protection of steel and R.C. structures at Enea-Casaccia shaking tables, published in Proceedings of the 13th World Conference on Earthquake Engineering. Vancouver, B.C., Canada, 2004 (Paper No. 846).

[21] G.S. Cheok, H.S. Lew, Seismic performance of 1/3 scale post-tensioned precast beam-column connectionsProceedings of the 4th US National Conference on Earthquake Engineering May 20–24, 1990, p. 757.

[22] G.S. Cheok, H.S. Lew, Performance of precast concrete beam-to-column connections subject to cyclic loading, PCI J. 36 (1991) 56–67.

[23] M.J.N. Priestley, G.A. MacRae, Seismic tests of precast beam-to-column joint subassemblages with unbonded tendons, PCI J. 41 (1996) 64–80.

[24] M.J.N. Priestley, Myths and Fallacies in Earthquake Engineering, Revisited, IUSS Press, Pavia, Italy, 2003.

[25] J.M. Ricles, R. Sause, M.M. Garlock, C. Zhao, Posttensioned seismic-resistant connections for steel frames, J. Struct. Eng. 127 (2001) 113–121.

[26] C. Christopoulos, A. Filiatrault, C.-M. Uang, B. Folz, Posttensioned energy dissipating connections for moment-resisting steel frames, J. Struct. Eng. 128 (2002) 1111–1120.

[27] D. Wang, A. Filiatrault, Numerical and Experimental Studies of Self-Centering Post-Tensioned Steel Frames, MCEER, Buffalo, NY, 2008.

[28] C. Christopoulos, R. Tremblay, H.-J. Kim, M. Lacerte, Self-centering energy dissipative bracing system for the seismic resistance of structures: Development and validation, J. Struct. Eng. 134 (2008) 96–107.

[29] R. Tremblay, M. Lacerte, C. Christopoulos, Seismic response of multistory buildings with self-centering energy dissipative steel braces, J. Struct. Eng. 134 (2008) 108–120.

[30] M. Speicher, R. DesRoches, R.T. Leon, Analytical Study of SDOF Systems with Superelastic Shape Memory Alloy Properties, Proceedings of 18th Analysis and Computation Speciality Conference - Structures Congress 2008: Crossing the Borders, American Society of Civil Engineers, Vancouver, BC, Canada, 2008.

[31] M.R. Eatherton, X. Ma, H. Krawinkler, D. Mar, S. Billington, J.F. Hajjar, et al., Design concepts for controlled rocking of self-centering steel-braced frames, J. Struct. Eng. 140 (2014) (United States).

[32] D. Roke, R. Sause, J.M. Ricles, N. Gonner, Design concepts for damage-free seismic-resistant self-centering steel concentrically braced frames, 2009 Structures Congress - Don't Mess with Structural Engineers: Expanding Our Role, April 30, 2009-May 2, 2009, American Society of Civil Engineers, Austin, TX, United States 2009, pp. 1421–1430.

[33] L. Wiebe, Design and construction of controlled rocking steel braced frames in New Zealand, Improving the Seismic Performance of Existing Buildings and Other Structures, 2015, 2015, pp. 810–821.

[34] MANSIDE, Memory Alloys for New Structural Vibrations Isolating Devices, Italian Dept. for National Technical Services, Rome, 1998.

[35] M. Dolce, D. Cardone, Theoretical and experimental studies for the application of shape memory alloys in civil engineering, J. Eng. Mater. Technol. Trans. ASME. 128 (2006) 302–311.
[36] M. Dolce, D. Cardone, R. Marnetto, Implementation and testing of passive control devices based on shape memory alloys, Earthq. Eng. Struct. Dyn. 29 (2000) 945–968.
[37] M. Dolce, D. Cardone, R. Marnetto, SMA Re-centering devices for seismic isolation of civil structures, Smart Systems for Bridges, Structures, and Highways-Smart Structures and Materials 2001-, Mar 5–7 2001, Society of Photo-Optical Instrumentation Engineers, Newport Beach, CA 2001, pp. 238–249.
[38] M. Dolce, D. Cardone, R. Marnetto, M. Mucciarelli, D. Nigro, F.C. Ponzo, et al., Experimental static and dynamic response of a real R/C frame upgraded with SMA re-centering and dissipating braces, published in the Proceedings of the 13th World Conference on Earthquake Engineering. Vancouver, B.C., Canada, 2004.
[39] M. Dolce, D. Cardone, F.C. Ponzo, C. Valente, Shaking table tests on reinforced concrete frames without and with passive control systems, Earthq. Eng. Struct. Dyn. 34 (2005) 1687–1717.
[40] M. Dolce, R. Marnetto, Seismic Devices Based on Shape Memory Alloys, Manside Project: Italian Dept. for National Technical Services, Rome, Italy, 1999.
[41] R. DesRoches, J. McCormick, M. Delemont, Cyclic properties of superelastic shape memory alloy wires and bars, J. Struct. Eng. ASCE 130 (2004) 38–46.
[42] J. McCormick, J. Tyber, R. DesRoches, K. Gall, H.J. Maier, Structural engineering with NiTi. II: Mechanical behavior and scaling, J. Eng. Mech. 133 (2007) 1019–1029.
[43] S. Zhu, Y. Zhang, Seismic analysis of concentrically braced frame systems with self-centering friction damping braces, J. Struct. Eng. 134 (2008) 121–131.
[44] M. Speicher, D.E. Hodgson, R. Desroches, R.T. Leon, Shape memory alloy tension/compression device for seismic retrofit of buildings, J. Mater. Eng. Perform. 18 (2009) 746–753.
[45] D.J. Miller, L.A. Fahnestock, M.R. Eatherton, Development and experimental validation of a nickel–titanium shape memory alloy self-centering buckling-restrained brace, Eng. Struct. 40 (2012) 288–298.
[46] J. Ocel, R.T. Leon, R. DesRoches, R. Krumme, J.R. Hayes, S. Sweeney, Full-Scale Testing of Nitinol-Based Semi-Rigid Connections, published in the Proceedings of the 12th Conference on Earthquke Engineering, London, UK, 2002.
[47] J. Sepulveda, R. Boroschek, R. Herrera, O. Moroni, M. Sarrazin, Steel beam-column connection using copper-based shape memory alloy dampers, J. Constr. Steel Res. 64 (2008) 429–435.
[48] R. DesRoches, B. Taftali, B.R. Ellingwood, Seismic performance assessment of steel frames with shape memory alloy connections. Part I — analysis and seismic demands, J. Earthq. Eng. 14 (2010) 471–486.
[49] M.S. Speicher, R. DesRoches, R.T. Leon, Experimental results of a NiTi shape memory alloy (SMA)-based recentering beam-column connection, Eng. Struct. 33 (2011) 2448–2457.
[50] Y. Adachi, S. Unjoh, Development of shape memory alloy damper for intelligent bridge systems, published in Proceedings of SPIE Conference on Smart Systems for Bridges, Structures, and Highways. Newport Beach, CA 1999, pp. 31–42.
[51] B. Andrawes, R. DesRoches, Unseating prevention for multiple frame bridges using superelastic devices, Smart Mater. Struct. 14 (2005) 60–67.
[52] M.A. Youssef, M.S. Alam, M. Nehdi, Experimental investigation on the seismic behavior of beam-column joints reinforced with superelastic shape memory alloys, J. Earthq. Eng. 12 (2008) 1205–1222.
[53] AISC, Seismic Provisions for Structural Steel Buildings, American Institute of Steel Construction, Chicago, IL, 2005.
[54] P. Clark, K. Frank, H. Krawinkler, R. Shaw, Protocol for Farbrication, Inspection, Testing, and Documentation of Beam-Column Connection Tests and Other Experimental Specimens. SAC Steel Project Background Document, 1997.
[55] A.K. Chopra, Dynamics of Structures: Theory and Applications to Earthquake Engineering, third ed. Pearson/Prentice Hall, Upper Saddle River, N.J., 2007
[56] FEMA, NEHRP Recommended Provisions: Design Examples, 2006 Rep No FEMA 451. Washington, D.C.
[57] F. McKenna, G.L. Fenves, OpenSees Command Language Manual. Version 1.5.2, Pacific Earthquake Engineering Research Center, Berkeley, CA, 2004.
[58] F. Auricchio, E. Sacco, A one-dimensional model for superelastic shape-memory alloys with different elastic properties between austenite and martensite, Int. J. Non Linear Mech. 32 (1997) 1101–1114.
[59] D. Fugazza, Shape-Memory Alloy Devices in Earthquake Engineering: Mechanical Properties, Constitutive Modeling and Numerical Simulations [Master's Thesis], University of Pavia, Pavia, Italy, 2003.
[60] P. Somerville, N. Smith, S. Punyamurthula, J. Sun, Development of Ground Motion Time Histories for Phase 2, SAC Joint Venture, Sacramento, CA, 1997.